05,10

Shift of resonance frequencies of Stokes and anti-Stokes lines in Mandelstam-Brillouin spectra with changing interface in NiFe/Spacer/IrMn exchange-biased thin films

© M.V. Bakhmetiev[1], A.V. Sadovnikov[2], V.A. Gubanov[2], V.V. Savin[3], R.B. Morgunov[1,4,¶]

[1] Federal Research Center of Problems of Chemical Physics and Medicinal Chemistry RAS, Chernogolovka, Russia
[2] Saratov State University, Saratov, Russia
[3] Immanuel Kant Baltic Federal University, Kaliningrad, Russia
[4] Tambov State Technical University, Tambov, Russia
¶ E-mail: spintronics2022@yandex.ru

Received April 30, 2025
Revised May 15, 2025
Accepted May 25, 2025

Spin-waves in NiFe/Cu/IrMn and NiFe/Ta/IrMn heterostructures with variable thickness of copper and tantalum interlayers were studied by Brillouin Light Scattering (BLS). Resonance frequencies of the Stokes and anti-Stokes lines shift upon inversion of the external magnetic field. When the percolation threshold is reached in the interlayer, the sign of the frequency shift changes and remains negative until a continuous coating is achieved. Complete rupture of the direct exchange contact between the NiFe and IrMn layers by the non-magnetic material of the interlayer leads to a zero shift of the resonant scattering frequencies. Changes in the resonant frequencies of spin-wave scattering characterize the quality of the NiFe/Spacer/IrMn interface, the fractal dimension of which corresponds to the three-dimensional structure..

Keywords: Exchange bias, spacer, Mandelstam-Brillouin scattering spectra, shift of scattering resonance frequencies.

DOI: 10.61011/PSS.2025.06.61691.104-25

1. Introduction

Exchange bias effect is a fundamental interface property that occurs at the ferromagnetic (F) — antiferromagnetic (AF) interface. This effect is in that the spin interaction between the F and AF layers at the F-AF interface and the AF layer magnetization near the interface [1,2] cause a shift of the center of hysteresis loop with respect to a zero field. The effective field (exchange bias field H_{ex}) is directed along the residual magnetization of the F layer [1,3]. Extensive experimental and theoretical investigations over the years show that this effect is important for the development of magnetoelectronic devices. Ferromagnetic and antiferromagnetic spin dynamics in a magnetic field, and electrical transport phenomena accompanying reorientation of these spins are quite important for antiferromagnetic spintronic technologies [3–5].

There are three approaches to exchange bias adjustment at the F|AF thin film formation stage: F thickness variation [6], AF thickness variation [7] and introduction of a nonmagnetic NM interlayer between F and AF [8–10]. The first two approaches lead to considerable changes of thin film conductivity and only the latter, introduction of a very thin interlayer at the interface between the F and AF layers, makes it possible to maintain the structure conductivity at the same level [11] due to island formation of the nonmagnetic interlayer with thickness below the percolation threshold [12]. Therefore, introduction of nonmagnetic interlayer is a most effective exchange bias control method that is widely used in data storage and measuring devices [11].

At a certain thickness of the interlayer between the F and AF layers, a percolation threshold (infinite fractal) appears [13]. The percolation threshold is addressed in percolation theory and is associated with a special type of phase transition [14]. It takes a form of sudden change of material properties when the admixture concentration increases. To describe the appearance of a conductivity jump and formation of the infinite fractal in conductor-insulator composite materials [15], a lot of theoretical models may be used. Conductivity behavior in such composite materials is a complex function of particle concentration, sizes, shape, geometrical arrangement and other factors [16]. An empirical model based on the combination of mean-field theory and percolation theory is generally applied to cellular and colloidal systems [17,18]. This method is used directly for conductivity investigations, however, its utilization for the analysis of magnetic properties is rather phenomenological in nature and requires additional justifications and experimental evidence. In addition, introduction

of an interlayer into the NiFe|IrMn interface and increase in its concentration induces formation of a two-dimensional structure consisting of contacting Cu or Ta interlayer islands and when the required interlayer island concentration is achieved, the infinite fractal appears [14]. In our previous work [13], percolation theory was successfully applied to conductivity and magnetic properties of the NiFe|Cu|IrMn heterostructures.

Since the exchange bias field in the F|NM|AF structures affects the whole range of various properties associated with spin configurations at the interface, introduction of the interlayer and variation of the interlayer thickness between F and AF may be expected to change the Brillouin light scattering (BLS) spectra. It is reported in [19–21] that the exchange bias may affect the BLS spectra considerably. At least three mechanisms are known from the literature and can explain the influence of the exchange bias on the BLS spectra in the NiFe|IrMn structures: 1) change of thermal population of magnon energy levels after redistribution by the exchange bias field, 2) change of anisotropy field leading to resonance frequency shift in the BLS spectra, and 3) change of the off-diagonal spin operator components S_xS_y induced by magnetization vector rotation in the ferromagnetic film [19].

This study uses the BLS method to identify changes of the exchange bias caused by the Ta and Cu interlayer introduction into the NiFe|IrMn interface in a wide thickness range covering three interlayer growth stages: 1) island structure formation; 2) percolation structure formation and 3) continuous thin layer formation. Interference of direct and back spin waves propagating in opposite directions in the ferromagnetic material, NiFe, changes resonance frequencies depending on the interlayer growth stage.

2. Procedure and samples

Three types of samples were used for the study: type 1 without Ta(5 nm)|NiFe(11 nm)|IrMn(9 nm)|Ta(4 nm)|Ta_2O_5(2 nm) interlayer, type 2 with a tantalum interlayer between the NiFe and IrMn, Ta(5 nm)|NiFe(11 nm)|Ta(t_{Ta})|IrMn(9 nm)|Ta(4 nm)|Ta_2O_5(2 nm) layers with different tantalum layer thicknesses $t_{Ta} = 0.1, 0.15, 0.2, 0.25, 0.3, 0.5$, 1.0, 1.5 nm; and type 3 — with copper interlayer, Ta(5 nm)|NiFe (11 nm)|Cu (t_{Cu})|IrMn (9 nm)|Ta (4 nm)|Ta_2O_5 (2 nm) with different layer thicknesses $t_{Cu} = 0.1$, 0.2, 0.3, 0.4, 0.5, 0.6, 0.7, 0.8, 0.9, 1.0, 1.3, 2.0, 2.5, 5.0 nm. The samples were fabricated by direct current magnetron sputtering at a base pressure of $2.6 \cdot 10^{-7}$ mTorr, argon pressure of 3 mTorr and gas flow velocity of 30 cm^3 min. Sample fabrication procedure is similar to that described in [22]. During sample fabrication, interlayer sputtering time was varied gradually at the same sputtering rate. For tantalum interlayer, this time is from 2 to 30 s, and for the copper interlayer, this time is from 2 to 120 s. Since these two materials have different adhesion to the NiFe layer, the corresponding sputtering time was selected. Then the prepared samples were measured on the SQUID magnetometer that was used to determine the exchange bias field and coercive force. Percolation theory applicable to these magnetic properties was used to determine the percolation threshold for the NiFe|Cu|IrMn and NiFe|Ta|IrMn structures, when sudden decrease in the exchange bias field and coercive force occurred as described in [13]. The percolation threshold appears at the effective thickness for the copper interlayer $t_{Cu} = 0.5$ nm, and for the tantalum interlayer $t_{Ta} = 0.15$ nm. The continuous layer was determined by the change of structure resistance [13]. The interlayer resistance doesn't change until the continuous interlayer is formed. When $t_{Cu} = 1.3$ nm and $t_{Ta} = 0.3$ nm have been achieved, the structure resistance starts changing. In addition, the Monte Carlo method may be used for theoretical calculation of continuous layer formation for different interlayer materials by selecting the coefficients of interlayer adhesion to NiFe as shown in [23].

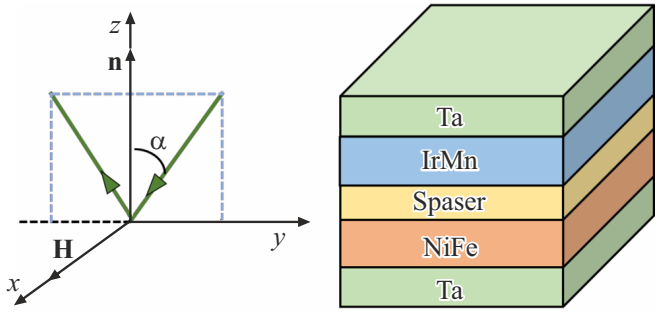

Figure 1. Scheme of the experiment for BLS spectra recording, **H** is the external magnetic field, α is the angle of laser beam incidence, **n** is the normal.

The effective interlayer thickness implies the amount of deposited interlayer material typical for one atomic layer and corresponding to an adequate amount of atoms for uniform atom distribution and full coverage of the NiFe|IrMn interface. In fact, this situation never takes place because islands consisting of 2-3-4, etc., layers are formed at such amount of atoms, so a part of the interface is not covered. The effective interlayer thickness was determined by the exchange bias field and theoretically predicted according to the sputtering time during heterostructure formation.

Light scattering spectra were measured by the BLS method at room temperature in the Damon–Eshbach geometry with laser beam back scattering (Figure 1). The external magnetic field H is oriented in the plane of the 5×5 mm^2 sample perpendicular to the plane of light incidence (Figure 1).

In the sample plane, the magnetic field was oriented in the direction, in which the exchange bias field identified by the independent measurements in the SQUID magnetometer was maximum (i.e. in the exchange bias field direction). The exchange bias field is maximum for the sample without interlayer and corresponds to $H_{ex} = 120$ Oe. As the effective interlayer thickness increases, the exchange bias field decreases and upon the achievement of $t_{Cu} = 1.3$ nm

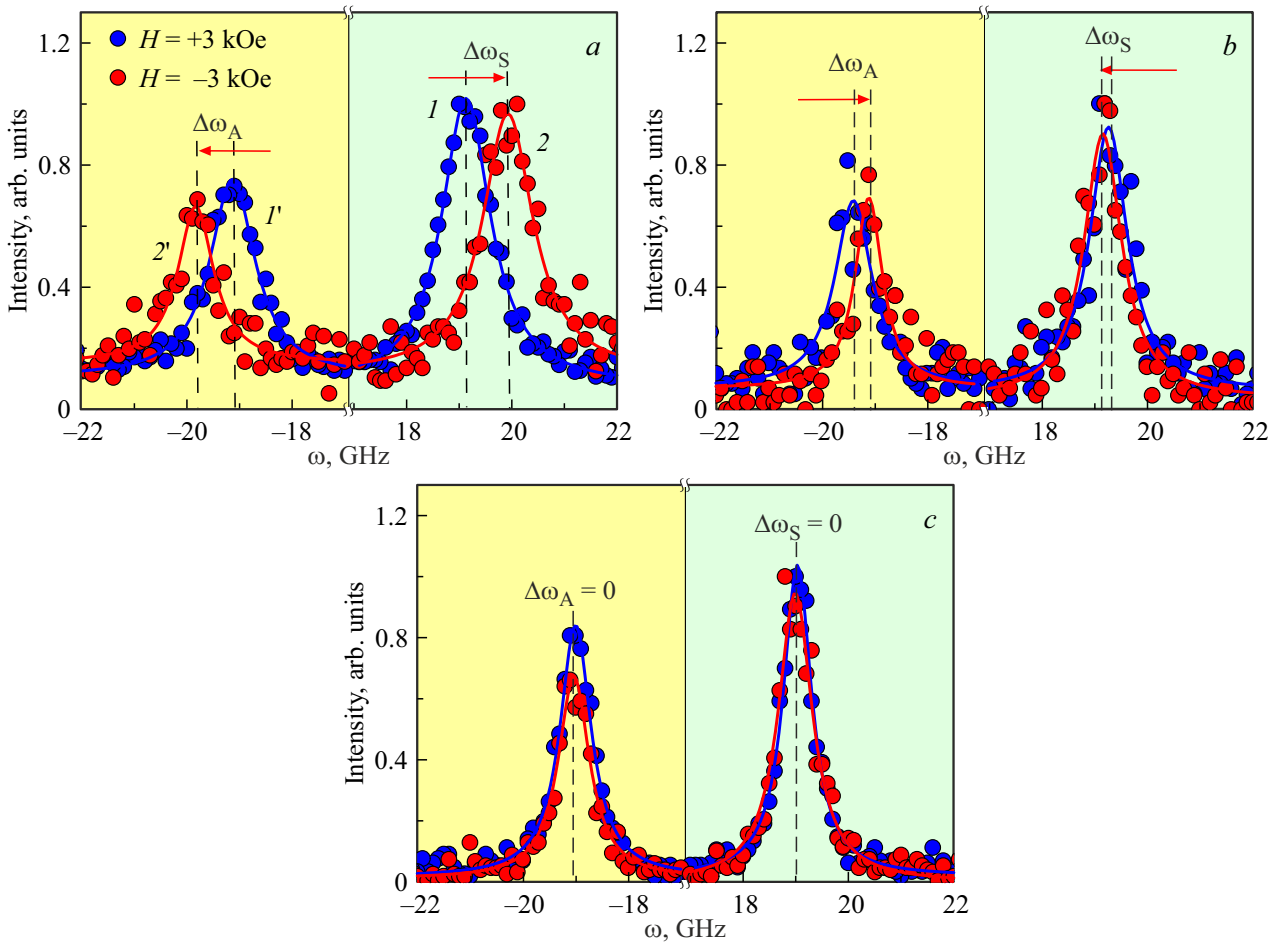

Figure 2. BLS spectra for NiFe|Cu|IrMn with external magnetic field inversion $H = \pm 3$ kOe *a*) for the interlayer thickness $t_{Cu} = 0.1$ nm; *b*) for the interlayer thickness $t_{Cu} = 0.5$ nm; *c*) for the interlayer thickness $t_{Cu} = 1.3$ nm.

and $t_{Ta} = 0.3$ nm becomes equal to zero [22] at room temperature indicating that a continuous interlayer has been achieved and the direct exchange contact has been broken. The BLS spectra were recorded in two external magnetic field orientations $H = +3$ kOe and $H = -3$ kOe with respect to the exchange bias field direction H_{ex} along the X axis in the sample. α was 15° with respect to the normal to the sample plane. For the BLS experiments, the external magnetic field is 3 kOe, i.e. is much higher than the exchange bias field. 3 kOe field means that the structure is in saturation where all ferromagnetic spins are co-directional with the external magnetic field. Selection of such external magnetic field implies that the system is in the expected state and will not make undesirable contributions to the experimental results.

3. Experimental results and discussion

Figure 2, *a* shows the BLS spectra for NiFe|Cu|IrMn with $t_{Cu} = 0.1$ nm with the external magnetic field inversion $H = \pm 3$ kOe. Similar BLS spectra were observed in NiFe|IrMn and NiFe|t_{Spacer}|IrMn for $t_{Ta} = 0.1$ nm and $t_{Cu} = 0.2$, 0.3, 0.4 nm where the island structure is formed and exists. At $H = +3$ kOe, there are Stokes (1) and anti-Stokes (1′) peaks that change their frequencies when the field is inverted $H = -3$ kOe and become lines (2) and (2′) (Figure 2, *a*). The observed shift of the Stokes and anti-Stokes line frequencies with the external magnetic field inversion is caused by the change of the effective field, including the external magnetic field and direct and indirect exchange interaction field between NiFe and IrMn.

To determine the Stokes and anti-Stokes line resonance frequency, the BLS spectra of the whole series of samples were approximated by the Lorentz function (solid lines in Figure 2). This made it possible to determine the centers of the lines and shifts $\Delta\omega_S$ and $\Delta\omega_A$. Magnetic field inversion leads to the Stokes peak shift by $\Delta\omega_S$ and to the anti-Stokes peak shift by $\Delta\omega_A$. These shifts are maximum for the sample without an interlayer and vary non-monotonously as the Cu and Ta layer thickness increases. Figure 2, *b* shows the BLS spectra for the sample $t_{Cu} = 0.5$ nm. The same BLS spectra are observed in NiFe|t_{Spacer}|IrMn for $t_{Ta} = 0.15$, 0.2, 0.25, 0.3 nm and $t_{Cu} = 0.6$, 0.7, 0.8, 0.9, 1.0 nm. Upon achievement of the percolation threshold (for $t_{Cu} = 0.5$ nm, for $t_{Ta} = 0.15$ nm),

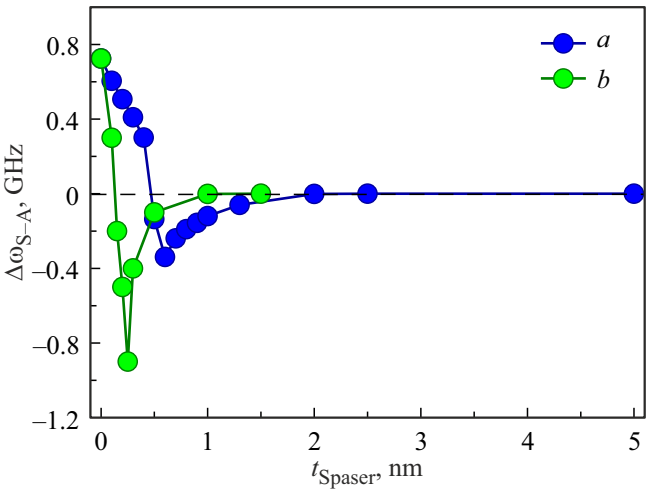

Figure 3. Dependence of $\Delta\omega_{S\text{-}A}$ on t_{Spacer} for *a*) NiFe|Cu|IrMn and *b*) NiFe|Ta|IrMn. Errors correspond to dot sizes.

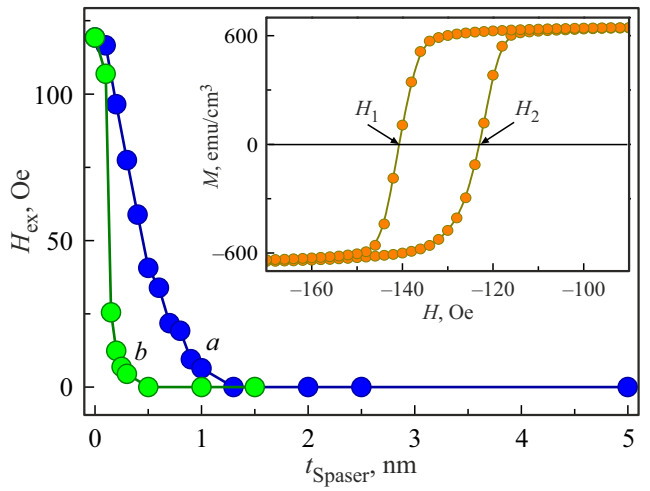

Figure 4. Dependence of the exchange bias field on t_{Spacer} for NiFe|Cu|IrMn (*a*) and NiFe|Ta|IrMn (*b*). Errors correspond to dot sizes. The inset shows the hysteresis loop for the NiFe|IrMn sample at $T = 300$ K with field designations H_1 and H_2. Magnetization is normalized to the NiFe volume $V = 2.5 \cdot 10^{-7}$ cm^3.

the sign of the Stokes and anti-Stokes peak shifts is reversed (Figure 2, *b*). Further increase in the interlayer thickness leads to a gradual decrease in the Stokes and anti-Stokes peak shifts to zero. Figure 2, *b* shows the BLS spectra for the sample $t_{Cu} = 1.3$ nm. The same BLS spectra are observed in NiFe|t_{Spacer}|IrMn for $t_{Ta} = 0.5$, 1.0, 1.5 nm and $t_{Cu} = 2.0$, 2.5, 5.0 nm. When the NiFe|IrMn interface is filled with the interlayer, effective thicknesses of Cu 0.5 nm and Ta 0.15 nm are sufficient for at least one continuous path to occur through copper or tantalum islands from one to the opposite end of the sample for percolation structure formation (infinite fractal). Formation of the infinite fractal leads to a sudden decease in the exchange bias field and coercive force [13].

The calculated $\Delta\omega_S$ and $\Delta\omega_A$ were averaged in a single data array and the mean shift $\Delta\omega_{S\text{-}A}$ was obtained. Figure 3 shows the dependence of $\Delta\omega_{S\text{-}A}$ on t_{Spacer} — effective Cu and Ta thickness. This parameter describes the amount of deposited interlayer material not only for the continuous layers, but also for the island structure and percolation network.

Effective thickness, at which the sign of $\Delta\omega_{S\text{-}A}$ is reversed both for NiFe|Cu|IrMn and NiFe|Ta|IrMn, coincides with the effective thickness, at which the percolation threshold appears for these structures. Magnon frequencies of spin waves propagating in the near-surface thin ferromagnetic layer are sensitive to formation of the infinite magnetic fractal at the interface.

Figure 4 shows the dependence of the exchange bias field on the effective Cu and Ta interlayer thicknesses.

This dependence was plotted according to equation $H_{ex} = |H_1 + H_2|/2$. As the effective Cu and Ta interlayer thickness grows, the direct exchange interaction between NiFe and IrMn decreases. It follows that the exchange bias field doesn't influence the sign reversal of $\Delta\omega_{S\text{-}A}$. The exchange bias field influences $\Delta\omega_S$ and $\Delta\omega_A$. Sign reversal of $\Delta\omega_{S\text{-}A}$ is possibly caused by the contribution of the indirect Rudermann–Kittel–Kasuya–Iosida (RKKI) exchange interaction through the Cu and Ta conductivity electrons. The energy of this interaction has an oscillating dependence on the distance between the interacting atoms. Amplitude of these oscillations and, consequently, the maximum values of the ferromagnetic and antiferromagnetic exchanges executed according to the RKKI mechanism increase with the spin-orbit interaction energy in the system. The difference in $\Delta\omega_{S\text{-}A}$ in Figure 3 between the Cu and Ta interlayers may be explained by different values of the spin-orbit interaction of Cu and Ta. It is well known that the presence of f-shell having high orbital moment in metals such as Pt, Ir, Ta, etc., enhances the exchange between magnetoresistive element layers due to a higher spin-orbit interaction energy compared with that of Cu, Ni, Fe, etc.

Thus, $\Delta\omega_S$ and $\Delta\omega_A$ with the external magnetic field inversion depends on the exchange bias field, sign reversal of $\Delta\omega_{S\text{-}A}$ depends on the indirect RKKI exchange interaction, and the effective thickness, at which the sign of $\Delta\omega_{S\text{-}A}$ is reversed, corresponds to the effective thickness, at which the infinite fractal appears.

4. Conclusion

It was found that the sign of the magnon frequencies of spin waves in the NiFe|Cu|IrMn and NiFe|Ta|IrMn structures is reversed when the effective nonmagnetic interlayer thickness achieves the percolation threshold. Gradual filling of the NiFe|Spacer|IrMn interface with interlayer atoms leads to a decrease in the shift of the Stokes and anti-Stokes line resonance frequencies, which corresponds to a monotonic decrease in the exchange bias field. Sign inversion of the resonance frequency shift direction disappears when the continuous interlayer is achieved. Magnon spin

wave frequency sing inversion depends on the formation of island interlayer bridges between the NiFe and IrMn layers in lateral direction as the interlayer thickness increases, and on the longitudinal irregularities in the NiFe layer. Magnetic dipole interaction between the NiFe film irregularities makes the interface structure equivalent to a three-dimensional magnetic fractal.

Funding

The study was supported by grant No. 22-19-20157 provided by the Russian Science Foundation (https://rscf.ru/project/22-19-20157/) and grant No. 11-C/2024 in the form of subsidy provided by the Government of Kaliningrad Oblast.

Conflict of interest

The authors declare no conflict of interest.

References

[1] R.L. Stamps. J. Phys. D: Appl. Phys. **34**, *3*, 444 (2001).
[2] P.K. Manna, S.M. Yusuf. Phys. Rep. **535**, *2*, 61 (2014).
[3] V. Baltz, A. Manchon, M. Tsoi, T. Moriyama, T. Ono, Y. Tserkovnyak. Rev. Mod. Phys. **90**, *1*, 015005 (2018).
[4] Y. Guo, Y. Ouyang, N. Sato, C.C. Ooi, S.X. Wang. IEEE Sensors **17**, *11*, 3309 (2017).
[5] A. Elzwawy, H. Pişkin, N. Akdoğan, M. Volmer, G. Reiss, L. Marnitz, A. Moskaltsova, O. Gurel, J.-M. Schmalhorst. J. Phys. D: Appl. Phys. **54**, *35*, 353002 (2021).
[6] S.M. Rezende, A. Azevedo, M.A. Lucena, F.M. de Aguiar. Phys. Rev. B **63**, *21*, 214418 (2001).
[7] R.L. Rodriguez-Suárez, L.H. Vilela-Leão, T. Bueno, A.B. Oliveira, J.R.L. Almeida, P. Landeros, S.M. Rezende, A. Azevedo. Phys. Rev. B **83**, *22*, 224418 (2011).
[8] L. Thomas, A.J. Kellock, S.S.P. Parkin. J. Appl. Phys. **87**, *9*, 5061 (2000).
[9] J. Sort, F. Garcia, B. Rodmacq, S. Auffret, B. Dieny. J. Magn. Magn. Mater. **272**−**276**, *Part 1*, 355 (2004).
[10] K. Li, Z. Guo, G. Han, J. Qiu, Y. Wu. J. Appl. Phys. **93**, *10*, 6614 (2003).
[11] A.D. Henriksen, G. Rizzi, M.F. Hansen. J. Appl. Phys. **119**, *9*, 093910 (2016).
[12] E. Byon, T.W.H. Oates, A. Anders. Appl. Phys. Lett. **82**, *10*, 1634 (2003).
[13] M.V. Bakhmetiev, A.D. Talantsev, R.B. Morgunov. JETP **132**, *5*, 852 (2021).
[14] C.-W. Nan, Y. Shen, J. Ma. Annu. Rev. Mater. Res. **40**, 131 (2010).
[15] I.J. Youngs. J. Phys. D: Appl. Phys. **35**, *23*, 3127 (2002).
[16] Q. Li, T. Li, J. Wu. J. Colloid Interface Sci. **239**, *2*, 522 (2001).
[17] N.I. Lebovka, S. Tarafdar, N.V. Vygornitskii. Phys. Rev. E **73**, *3*, 031402 (2006).
[18] D.S. McLachlan, C. Chiteme, W.D. Heiss, J. Wu. Physica B **338**, *1*−*4*, 261 (2003).
[19] P. Miltényi, M. Gruyters, G. Güntherodt, J. Nogués, I.K. Schuller. Phys. Rev. B **59**, *5*, 3333 (1999).
[20] C. Mathieu, M. Bauer, B. Hillebrands, J. Fassbender, G. Güntherodt, R. Jungblut, J. Kohlhepp, A. Reinders. J. Appl. Phys. **83**, *5*, 2863 (1998).
[21] R.L. Rodriguez-Suárez, A.B. Oliveira, F. Estrada, D.S. Maior, M. Arana, O. Alves Santos, A. Azevedo, S.M. Rezende. J. Appl. Phys. **123**, *4*, 043901 (2018).
[22] M. Bakhmetiev, A. Talantsev, A. Sadovnikov, R. Morgunov. J. Phys. D: Appl. Phys. **55**, *10*, 105001 (2022).
[23] R.B. Morgunov, M.V. Bakhmetiev, A.D. Talantsev. Phys. Solid State **62**, *11*, 1991 (2020).

Translated by E.Ilinskaya